Accepted Manuscript

The turn-off fluorescent sensors based on thioether-linked bisbenzamide for Fe^{3+} and Hg^{2+}

Hehong Lv, Ziqi Ren, Heng Liu, Ganbing Zhang, Hanping He, Xiuhua Zhang, Shengfu Wang

PII: S0040-4020(18)30165-0

DOI: 10.1016/j.tet.2018.02.031

Reference: TET 29302

To appear in: *Tetrahedron*

Received Date: 1 December 2017

Revised Date: 4 February 2018

Accepted Date: 14 February 2018

Please cite this article as: Lv H, Ren Z, Liu H, Zhang G, He H, Zhang X, Wang S, The turn-off fluorescent sensors based on thioether-linked bisbenzamide for Fe^{3+} and Hg^{2+}, *Tetrahedron* (2018), doi: 10.1016/j.tet.2018.02.031.

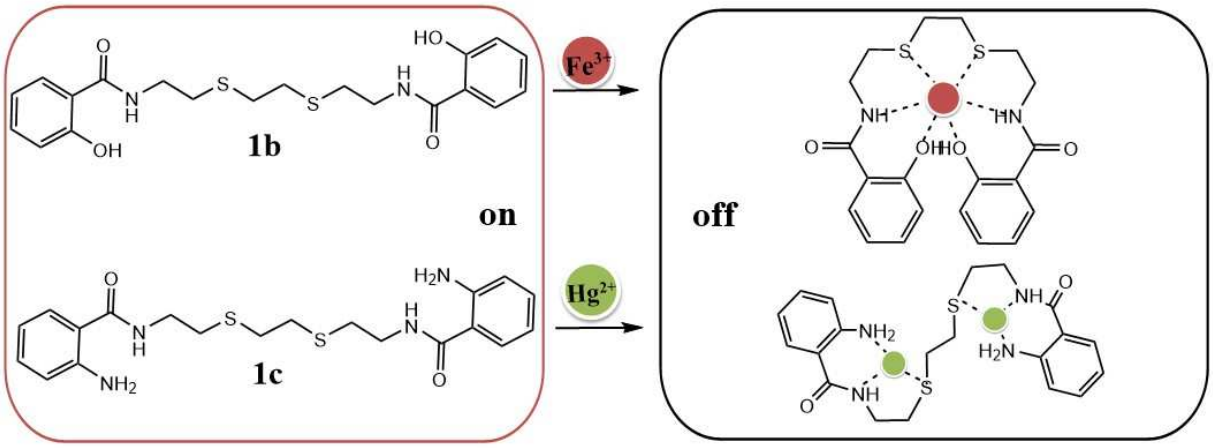

The turn-off fluorescent sensors based on thioether-linked bisbenzamide for Fe^{3+} and Hg^{2+}

Hehong Lv [b], Ziqi Ren [b], Heng Liu [a b], Ganbing Zhang* [a b], Hanping He*[a b], Xiuhua Zhang [a b], Shengfu Wang [a b]

a, Hubei Collaborative Innovation Center for Advanced Organic Chemical Materials; Hubei University, Youyi Road 368, Wuchang, Wuhan, Hubei 430062, (PR China).

b, Ministry of Education Key Laboratory for the Synthesis and Application of Organic Functional Molecules, College of Chemistry and Chemical Engineering, Hubei University, Youyi Road 368, Wuchang, Wuhan, Hubei 430062, (PR China)

* Corresponding Authors: hehanping@hubu.edu.cn; gbzhang@hubu.edu.cn

Tel: +86-027-50865319; fax: +86-027-88663043

Abstract

Some dibenzamide derivatives with a thioether linker were designed, synthesized and characterized. The specific responses to Hg^{2+} and Fe^{3+} were investigated by fluorescence. According to fluorescence titration, the Job plot, ^1H NMR, and ESI-mass analysis, the derivative with mono- hydroxyl substituent (**1b**) on the aromatic ring has high selectivity for Fe^{3+} ion with the formation of 1:1 **1b**-Fe^{3+} complexes. The specificity of **1c** for Hg^{2+} could be switched by swapping the substituent from hydroxyl to amino, and a 1:2 (**1c**-Hg^{2+}) complex was formed. Along with the obtained results, density functional theory (DFT) and natural bond orbital (NBO) analyses were employed to explore the geometric structures, properties and possible mechanisms.

Keywords: Fluorescent sensor; Metal ion; Fe^{3+}; Hg^{2+}; Bisbenzamide;

1. Introduction

Fluorescent sensors for metal ions have been widely applied not only in environmental monitoring but also in biological studies.[1-3] Especially in recent years, selective and sensitive detection of heavy and transition metal ions has been received considerable attention because these metals caused adverse health and environmental problems.[4-9] Particularly, Hg (II) was regarded as one of the most toxic metal ions. Due to its accumulative and highly toxic character, mercury can cause serious health problems like prenatal brain damage, cognitive and motion disorder, minamata diseases, etc.[10-12] Fe (III) is an essential trace element in fundamental physiological processes, being indispensable for all living systems. It performs the oxygen-carrying capacity of heme as well as acts as a cofactor in many enzymatic reactions.[13,14] However, its deficiency or overload has a toxic effect on living organisms and causes diseases such as anemia and hemochromatosis.[15,16] Because of these environmental and health problems of Hg^{2+} and Fe^{3+}, designing highly selective and sensitive chemosensors for these two metals has been still a challenge.

Up to now, significant progress was achieved in the selective detection of Hg^{2+} and Fe^{3+}.[17-27] Most of them were based on different organic molecular systems/materials that included azo-derivatives[17,25,20], crown-ethers[24,26], naphthalimide[19], anthraquinone[21], rhodamine[23,18], benzothiazole[27], BODIPY[25,26] and so on. Among these ion recognition units, crown ethers-based chemosensors were widely used due to their advantageous characteristics: the ability to coordinate the cations of alkaline metals, high selectivity and accessibility. So far, Crown ether derivatives incorporating a fluorescent moiety have been attractive tools for optical sensing of all kinds of ions, such as Hg^{2+}, Fe^{3+}, Ag^{+}, Pb^{2+}.[28] In 2008, Zhu et al. designed a novel dye containing dithia-dioxa-monoaza crown ether moiety that can perform highly sensitive detection of Hg^{2+} ion in the NIR region.[29] In 2014, Sui et al. presented a new Fe^{3+}-recognizing cryptand with high selectivity, sensitivity, and reversibility toward Fe^{3+} detection.[30] However, for most fluorescent sensors of Hg^{2+} and Fe^{3+}, a common limitation is that they are rather complicated, delayed response to

the ion, and that their analytical results are easily influenced by coexisting ions.[9] Additionally, most of sensors only worked well in the organic medium due to their poor aqueous solubility. Therefore, development of fluorescent sensors with more sensitivity, reliability, and aqueous medium solubility is in high demand for the detection of Fe^{3+} and Hg^{2+}.

In addition, podands linked different fluorescein are also used to identify various kinds of metal. Chang group previously reported a series of copper-responsive indicators containing both BODIPY and the double ethanedithiol units.[31,32] Nolan and co-workers synthesized a fluorescent sensor based on polioxo ethylene chain, which was used with alkaline earth cations was examined.[33] Inspired by these concepts, we have focused our interest on designing simple molecules which could serve as receptors to recognize Fe^{3+} based on a fluorescence 'on-off' mechanism. Herein we synthesized some ethanedithiol derivatives **1a-g** (**Scheme 1**) with two substituted benzamide units for detecting Fe^{3+} and Hg^{2+} ions in aqueous solution. The chelating groups like carbonyl and carboxamide had high binding affinity to transition metal ions in comparison with alkali and alkaline earth metal ions. Furthermore, the ethanedithiol linker is flexible, which is helpful to chelate Hg^{2+} and Fe^{3+} ions.[34] In this work, the changes of substituent groups on the benzene ring ortho of **1** significantly altered the fluorescence response toward the metal ions. To our surprise, compared to other six sensors, **1b** with hydroxyl substituent showed remarkable selective response toward Fe^{3+}. **1c** with amine enhanced the selectivity for Hg^{2+} ions over Fe^{3+} ions, when the hydroxyl is replaced with amino.

2. Results and discussion

2.1 Synthesis

The compounds **1a-1g** featured with the thioether linker and dibenzamide units. Their synthetic pathways were similar (as shown in **Scheme 1)**. Compound **2** was readily obtained by the reaction of cysteamine hydrochloride and1,2-dibromoethane in ethanol with a satisfied yield of 71%. Compound **2** was then reacted with different substituents of benzoic acid derivatives to give **1a,1b,1c,1d,1e,1f**,**1g**, respectively. The

chemical structures of compounds **2** and **1a-1g** were characterized by ^{1}H NMR, ^{13}C NMR and ESI-MS (**Fig. S1–S24**, Supplementary data).

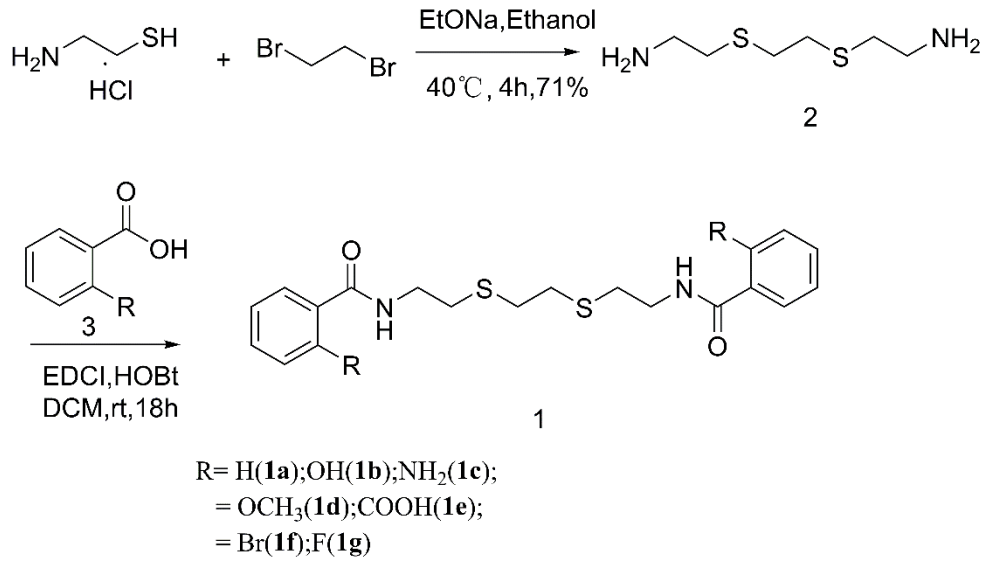

Scheme 1 Synthesis route to compounds **1a-1g.**

2.2 Spectral studies and specificity of **1a-1g** to metal ions

At first, the binding of probes **1a-1g** with metal ions was investigated by fluorescence spectroscopic measurements in DMSO/H_2O (5:95; v/v) mixed solution. As shown in **Fig. 1** and **Fig. S25**, the probes (10μM) exhibited better fluorescence. Particularly, the 10μM free ligands **1b, 1c** and **1d** with electron-donating groups exhibited higher fluorescence emission intensities on excitation at 297, 317 and 290nm, respectively. On the contrary, **1a, 1e, 1f** and **1g** with electron-accepting groups showed lower fluorescence emission intensities. The interaction of all the probes and various ions were investigated by fluorescence spectra. In the presence of excess metal ions (100 μM), it was found that the addition of Fe^{3+} into the receptors solution resulted in a varying decrement of fluorescence for free receptors **1a-1g**. Especially for probe **1b**, the fluorescence was almost quenched completely. The result indicated the probe **1b** exhibited an excellent selectivity for Fe^{3+}. Similarly, probe **1c** had good selectivity for Hg^{2+} as shown in **Fig. 1**. Pleasantly, for other ions including Na^{+}, K^{+}, Cu^{2+}, Fe^{2+}, Ba^{2+}, Mg^{2+}, Mn^{2+}, Ca^{2+}, Cr^{3+}, Ni^{2+}, Pb^{2+}, Zn^{2}+, Co^{2+} and Cd^{2+}, the receptors (**1a-1g**) showed no apparent fluorescence intensity alternation. In addition, other +3 cations (such as Tm^{3+}、Gd^{3+}、Y^{3+}、Sc^{3+} and La^{3+}) didn't interfere the

fluorescent emission (Fig. S26).

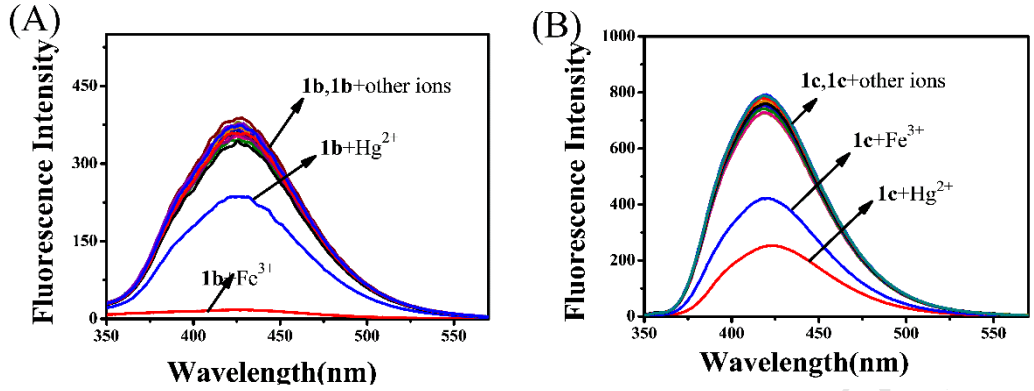

Fig. 1. Fluorescence emission spectra of **1b** (A) and **1c** (B) (10μM) in the presence of 10.0 equiv. of different metal ions (Na^+,K^+,Mn^{2+},Mg^{2+},Ca^{2+},Cr^{3+},Fe^{3+},Ni^{2+},Cu^{2+},Zn^{2+},Co^{2+},Ag^+,Cd^{2+},Hg^{2+},Fe^{2+} and Pb^{2+}) in DMSO/H_2O (5:95, v/v).

The detail fluorescence changes of the probes in the presence of Fe^{3+} and Hg^{2+} were analyzed as shown in **Fig. 2**. Here, the value of F/F_0 was used to represent fluorescence quenching degree, where F and F_0 represent the fluorescence intensity in the presence and absence of metal ions respectively. Although the fluorescence of these probes was quenched some certain after addition of Fe^{3+}, quenching of probe **1b** was most (F/F_0 = 0.04791) compared to other six probes. When the interactions of these probes and Hg^{2+} were analyzed, probe **1c** with amine substituent exhibited most binding to Hg^{2+} interestingly. The quenching was also studied using some different excitation wavelengths (260, 280, 330, 350nm) again in a broad range. It was found that the fluorescence was similarly quenched by the addition of Fe^{3+} or Hg^{2+} (as shown in Fig. S27). The photos obviously showed the quenching (as shown in Fig.2B and 2C). We didn't find obvious color changes in 1b or 1c solution when metal ions were added. The data of UV-vis spectrometry (Figure S28) also showed that no significant changes were observed even in the presence of Fe^{3+} or Hg^{2+}. A small hyperchromicity was observed for 1b, the intensity of absorption peak was decreased for 1c.

Further, the corresponding photoluminescence quantum yield of **1b** and **1c** was investigated for the quenching. The fluorescence quantum yield of **1b** decreased from 0.329 to 0.147 in the absence or presence of 10 eq. Fe^{3+}. And the fluorescence

quantum yield of **1c** decreased from 0.951 to 0.29 in the absence or presence of 10 eq. Hg^{2+}. These results indicated that probe **1b** with hydroxyl group had excess specificity to Fe^{3+}, and probe **1c** with amine group showed very good specificity to Hg^{2+} over other competitive metal ions. In addition, the fluorescence lifetime were 6.13 ns, 3.26 ns, 2.81 ns, and 3.53 ns for 1b, 1c, 1b–Fe^{3+} and 1c-Hg^{2+} complex, respectively. These are very important for understand the emission nature of complexes.

Another issue was whether pH of test solution would affect the selectivity and sensitivity of the sensors. The acid titration experiments were examined at a pH range from 3.0 to 12.0 in DMSO-H_2O (v/v = 5/95) solution. As displayed in **Fig.S29,** there were no noticeable change in the fluorescence intensity for both free **1b** and **1b**–Fe^{3+} complex within the pH range 3.0–9.0. However, at basic pH (>9), a fluorescence increase was found for **1b** and **1b-Fe^{3+}** complex. For free **1b**, deprotonation of phenolic-OH may break down hydrogen bonded chelation and could enhance fluorescence emission. For **1b-Fe^{3+}** complex, the high pH would cause precipitation of ferric hydroxide. The fluorescence of **1c** was stable over a wide range of pH values (4.0-12.0). While the intensity of **1c-Hg^{2+}**complex gradually increased with increasing pH value, the quenching was also obvious in wide range (pH: 4.0-10.0). Overall, both 1b and 1**c** showed a highly selective fluorescence “turn-off” response in a wild pH range from 4.0 to 9.0.

Finally, it was found that the fluorescence signals became immediately weakened and arrived a stable value within 1 min (As shown in Figure S30), following the addition of 10 equiv. Fe^{3+} to 1b (10μM) and 10 equiv. Hg^{2+} ion to 1c (10μM). These illustrated that the reactions of 1b with Fe^{3+} and 1c with Hg^{2+} ware completed rapidly.

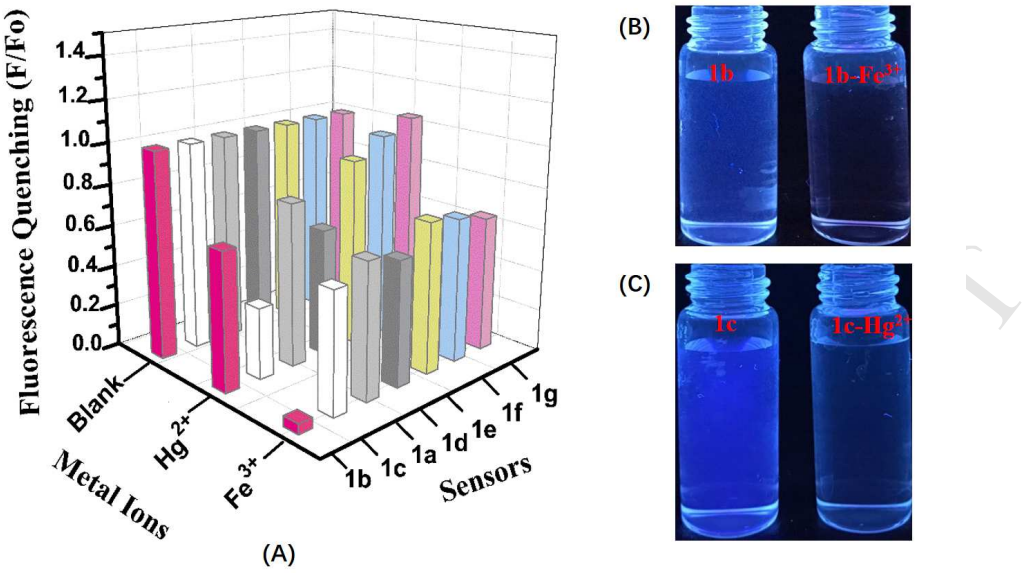

Fig. 2. (A) Selectivity of **1a**, **1b**, **1c**, **1d**, **1e**, **1f** and **1g** fluorescence response for Fe^{3+} and Hg^{2+}. F and F_0 represent the fluorescence intensity in the presence and absence of metal ions, respectively. (B) The sensor 1b under the UV lamp (365 nm) in the presence of Fe^{3+}. (C) The sensor 1c under the UV lamp (365 nm) in the presence of Hg^{2+}.

2.3 Interference studies

The above spectrum studies indicated that Fe^{3+} and Hg^{2+} lead to selectively fluorescence quenching of probe **1b** and **1c**, respectively. The interference must also be considering due to that there were mixture ions normally in practical samples. Here the interferences of other ions were further investigated, as shown in **Fig. 3A**. It was found that the fluorescence intensity of **1b** had no apparent changes in the presence of other metal ions including Na^{+}, K^{+}, Mn^{2+}, Mg^{2+}, Ca^{2+}, Cr^{3+}, Ni^{2+}, Cu^{2+}, Zn^{2+}, Co^{2+}, Ag^{+}, Cd^{2+}, Fe^{2+} and Pb^{2+}. Importantly, the strong fluorescence quenching was observed once there was Fe^{3+} in samples. Similarly, the fluorescence intensities of **1c** wasn't almost affected except that Fe^{3+} resulted in some quenching. Existence of Hg^{2+} ions made the strong fluorescence quenching to be observed. The selectivity of **1c** to Hg^{2+} ions were almost not influenced by the presence of other competing metal ions (**Fig. 3B**). Therefore, probes **1b** and **1c** was ability to be used as highly selective sensors for detections of Fe^{3+} and Hg^{2+}, respectively.

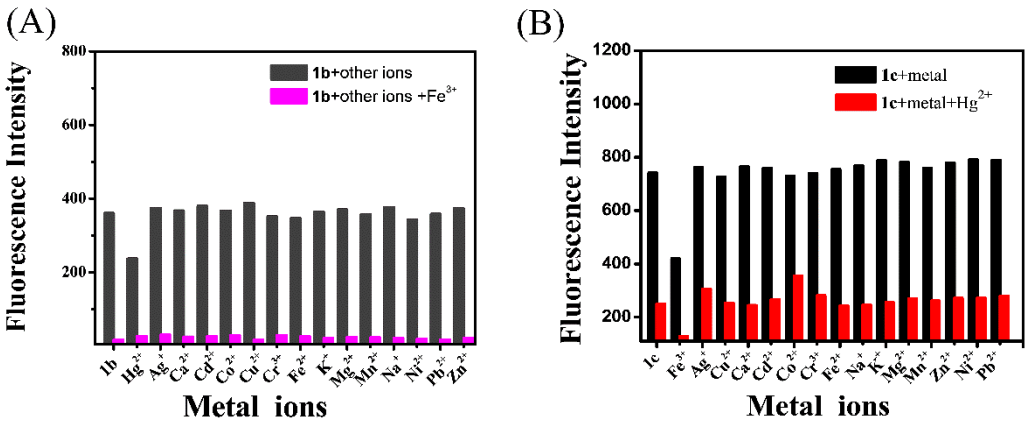

Fig. 3. (A) Metal ion selectivity profiles of **1b**(10μM): gray bars, fluorescence of **1b** in the absence and the presence of 10 equiv. of other compet*it*ion metal ions; pink bars, fluorescence of **1b** in the presence of 10 equiv. of various metal ions, followed by 10 equiv. of Fe^{3+}. (B) metal ion selectivity profiles of **1c** (10μM): black bars, fluorescence of **1c** in the absence and the presence of 10 equiv. of other competition metal ions; red bars, fluorescence of **1c** in the presence of 10 equiv. of various metal ions, followed by 10 equiv. of Hg^{2+}.

Besides, the interferences of various anions on Fe^{3+}-triggered and Hg^{2+}-triggered fluorescence quenching efficiency were also investigated respectively. As shown **Fig. 4A**, no obvious interferences were observed in presence of different anions including Br^-, Cl^-, F^-, CO_3^{2-}, HCO_3^-, HSO_3^-, NO_2^-, NO_3^-, $S_2O_3^{2-}$, SO_3^{2-}, SO_4^{2-} and CH_3COO^-. For Hg^{2+}-triggered fluorescence of **1c**, it was clearly shown that the quenching efficiency was not affected by some anions such as F^-, NO_2^-, NO_3^-, $S_2O_3^{2-}$, SO_3^{2-}, SO_4^{2-} and CH_3COO^- (in **Fig. 4B**). However, the Hg^{2+}-triggered quenching efficiency were affected by Br^-, Cl^-, HSO_3^-, HCO_3^{2-} and CO_3^{2-}. These were probably attributed to the form of the tetrahedral anion HgX_4^{2-} between HgX_2 (X = C1, Br, or I) with excess halide[35,36] and the form of precipitation between Hg^{2+} and HSO_3^-, HCO_3^{2-} and CO_3^{2-}.

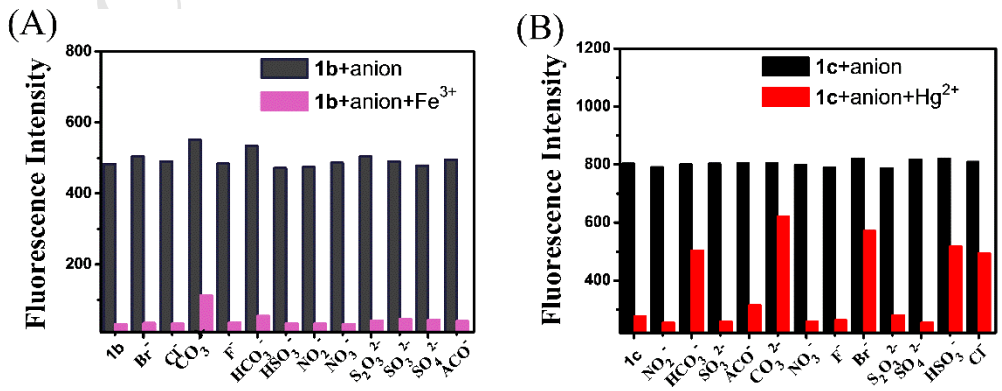

Fig. 4. (A) Fluorescence intensity of **1b** (10 μM) upon addition of Fe^{3+} (100 μM) in different anions (100 μM). **(B)** Fluorescence intensity of **1c** (10 μM) upon addition of Hg^{2+} (100 μM) in different anions (100 μM).

2.4 Fluorescence titration with metal ions

To further understand the binding behavior of **1b** and **1c** to Fe^{3+} and Hg^{2+} respectively, the fluorescence titrations were investigated in DMSO/H_2O (v/v = 5/95) solution. As shown in **Fig. 5A**, the fluorescence intensity decreased sharply with increasing concentration of Fe^{3+} ion ranging from 0 to 1.5 equiv. The relationship of fluorescence quenching and concentration ratio ([Fe^{3+}]/[**1b**]) was gave, which showed that the quenching tended to stable after the ratio of [Fe^{3+}]/[**1b**] was more than one. These results indicated that the 1:1 metal-ligand complex was probably formed between the probe **1b** and Fe^{3+} in DMSO/H_2O (5:95, v/v) solution. Importantly, a good linear relationship (y = -0.01044 + 1.13487x) observed between the fluorescence quenching efficiency and ratio of [Fe^{3+}]/[**1b**] in the range of 0–0.5 (**Fig. 5B**). Moreover, the limit of detection (LOD) was calculated to be 0.3 μM according to the reported method,[37] which was below the upper limit of Fe^{3+} level (about 5.357μM) in drinking water.[38] Similarly**,** the fluorescence intensity decreased obviously with the gradual titration of Hg^{2+} ion. The fluorescence quenching tended to be relative stable when the ratio of [Hg^{2+}]/[**1c**] was about 2, which indicated that the 2:1 metal-ligand complex was probably formed between the probe **1c** and Hg^{2+} in DMSO/H_2O (5:95, v/v) solution (**Fig. 6A**). A linear relationship (y = 0.00115 + 0.30578x) was observed between the fluorescence quenching efficiency and ratio of [Hg^{2+}]/[**1c**] in the range of 0-1.0 (**Fig. 6B**), and the detection limit was 0.5μM. Compared with previous methods (**Table S1**), probe **1b** and **1c** had the lower detection limit to Fe^{3+} and Hg^{2+},

respectively.

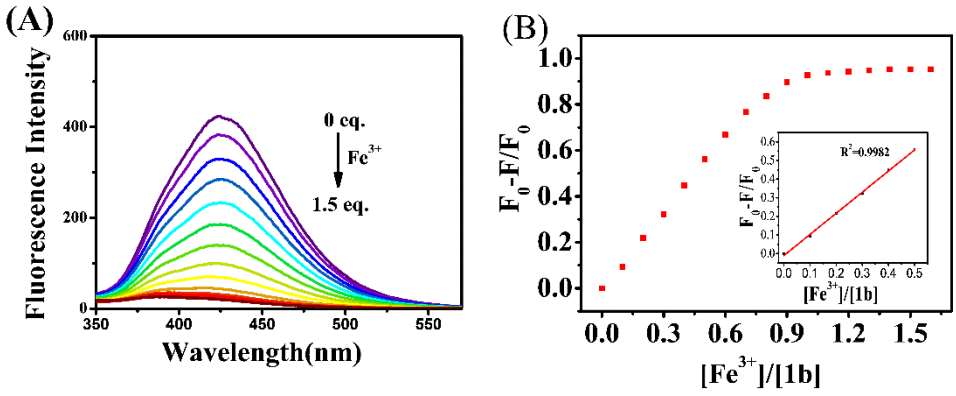

Fig. 5. (A) Fluorescence spectra of **1b** (10μM) upon the addition of different amounts of Fe^{3+} (0–1.5equiv) in DMSO/H_2O (5:95, v/v) solution, excitation and emission wavelengths were 297 and 426 nm, respectively. (B) The ratio of integrated fluorescence (F/F_0) of **1b** as a function of Fe^{3+}concentration. Inset: the linear relationship of **1b** between F_0-F/F_0 and Fe^{3+} concentration. F_0 and F represent the fluorescence intensities at 426 nm in the absence and presence of Fe^{3+}.

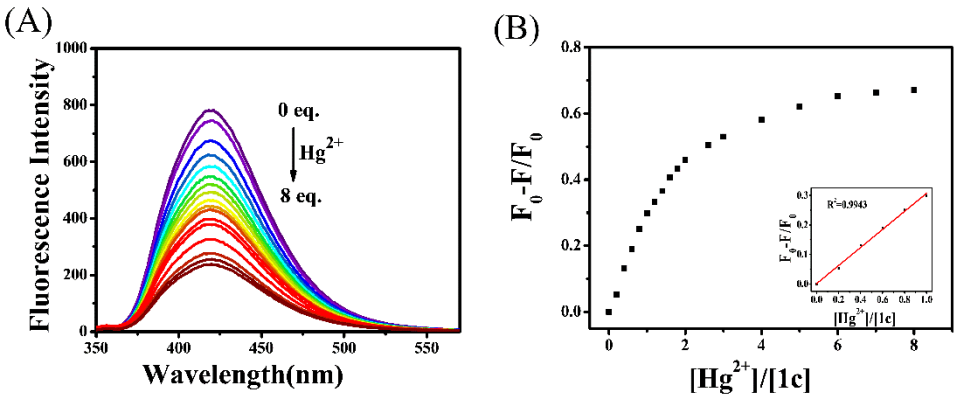

Fig. 6. (A) Fluorescence spectra of **1c** (10μM) upon the addition of different amounts of Hg^{2+} (0–8equiv) in DMSO/H_2O (5:95, v/v) solution, excitation and emission wavelengths were 317 and 419 nm, respectively. (B) The ratio of integrated fluorescence (F/F_0) of **1c** as a function of Hg^{2+}concentration. Inset: the linear relationship of **1c** between F/F_0 and Hg^{2+} concentration. F_0 and F represent the fluorescence intensities at 419 nm in the absence and presence of Hg^{2+}.

2.5 Binding Stoichiometry

Based on the above fluorescence titration, the complexes with 1:1 **1b**-Fe^{3+} and 1:2 **1c**-Hg^{2+} were probably formed respectively in DMSO/H_2O (5:95, v/v) solution. Here, a Job's Plot and ESI-MS were further constructed to determine the stoichiometry of binding. As shown **Fig. 7**, Job's plot obtained from the fluorescence

measurements showed 1:1 stoichiometric ratio for **1b**-Fe^{3+} complex, and 1:2 stoichiometric ratio **1c**-Hg^{2+} complex.

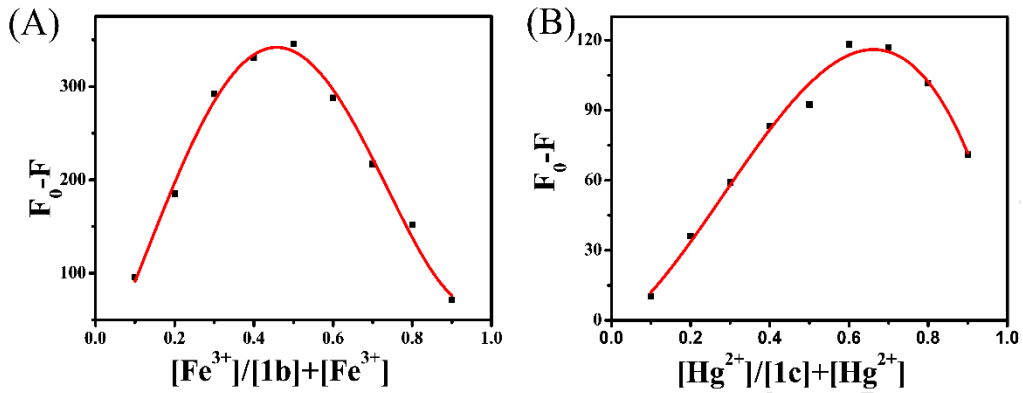

Fig. 7. Job's plots for the complexation of **1b** with Fe^{3+} (A) and **1c** with Hg^{2+} (B) in DMSO-H_2O (v/v = 5/95) solution.

The data were further confirmed by EIS-MS analysis. (As shown in **Fig. S31-S34** in supporting information). EIS-MS of **1b**-Fe^{3+} complex showed that a peak at m/z 474.1 that be assignable to [**1b**+Fe^{3+} -2H]$^+$ and a peak at m/z 551.7 that be assignable to [**1b**+Fe^{3+}+Cl^-+Na^++H_2O-H]$^+$ (**Fig. S31** and **Fig. S32**), which indicated that the 1:1 complex was formed. EIS-MS of complex **1c**-Hg^{2+} exhibited a peak at m/z =891.9, which corresponded to [**1c**+2Hg^{2+}+2Cl^-+2H]$^+$. The data were consistent with the above fluorescence titration and Job's Plot.

According to the above fluorescence titration and Job's plot, association constants were studied based on Benesi-Hildebrand equation (1),[39] where F_0 and F are the fluorescence intensities of the ligand in the absence and presence of the metal ion, respectively. F_{max} is the fluorescent intensity at a complete interaction concentration of the metal ion. K_a is the association constant, and n is binding stoichiometry ratio for the ligand and the metal ion. The association constant could (K_a) be determined by plotting 1/(F_0-F) against 1/[M]^n. And the association constants of **1b**-Fe^{3+} and **1c**-Hg^{2+} complexes were determined as 2.80 × 10^4 M^{-1} and 3.27 × 10^{10} M^{-2} respectively, assuming 1:1 stoichiometry for **1b**-Fe^{3+} and 1:2 stoichiometry for **1c**-Hg^{2+} (**Fig. 8A** and **Fig. 8B**).

$$\frac{1}{F_0-F} = \frac{1}{\{K_a\times(F_0-F_{max})\times[M^+]^n\}} + \frac{1}{F_0-F_{max}} \quad (1)$$

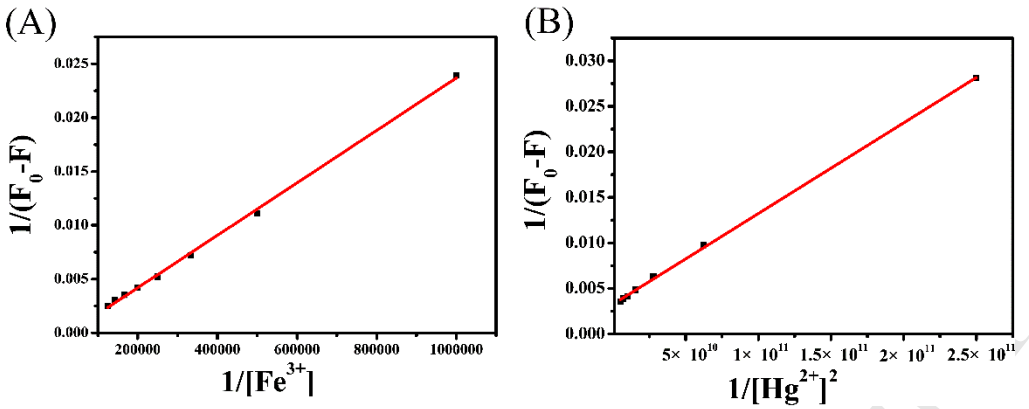

Fig. 8. Benesi–Hildebrand plots assuming 1:1 stoichiometry from Fluorometric titration data of receptor **1b** (10 μM) with Fe^{3+} (A) and 1:2 stoichiometry for receptor **1c** with Hg^{2+} (B).

2.6 The reversibility of fluorescence quenching

In order to observe whether the spectra of probes **1b** and **1c** could be regenerated upon the addition of cation-chelating agents, the reversibility of Fe^{3+} -triggered and Hg^{2+}-triggered quenching was performed with EDTA titration method.[40] As shown in **Fig. 9**, the fluorescence of probes **1b** and **1c** were not affected by the presence of EDTA. Fe^{3+}-triggered fluorescence quenching at 426 nm was recovered to 60% instantaneously after the addition of EDTA. Interestingly, further addition of 10 eq. of Fe^{3+} to the mixture solution again resulted in almost completely fluorescence quenching of probe **1b**. These indicated that the fluorescence probe **1b** detecting Fe^{3+} ion was reversible. The phenomenon was also observed for Hg^{2+}-triggered fluorescence system (**Fig. 9B**).

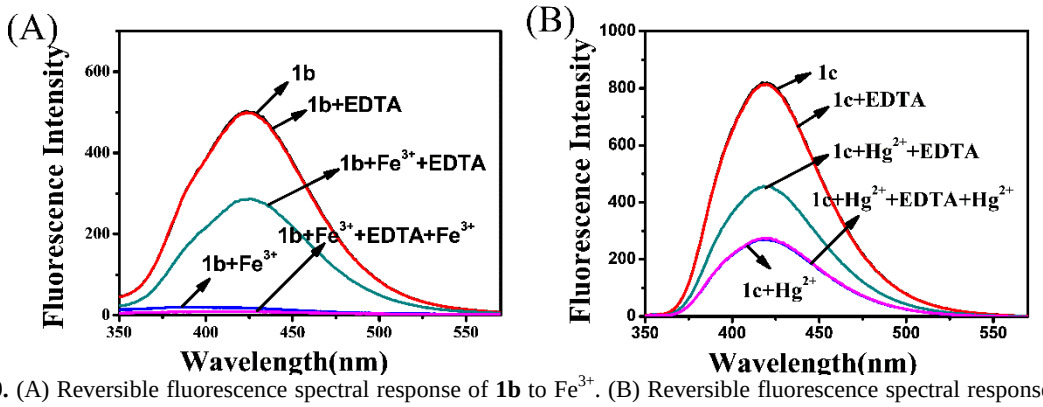

Fig. 9. (A) Reversible fluorescence spectral response of **1b** to Fe^{3+}. (B) Reversible fluorescence spectral response of **1c** to Hg^{2+}.

2.7 Possible recognition pattern

To further elucidate the sensing mechanism, ^{1}H NMR, FTIR spectrum and computational studies were investigated. ^{1}H NMR spectra of the probes **1b** and **1c**

were recorded in the absence and presence of metal ion (Note: the same D_2O was added when ^1H NMR of control sample was tested, because the solvent for the Fe^{3+} salt was heavy water). As shown in **Fig. 10**, the proton in phenolic-OH (**H1**) was at down-shifted from δ 12.48 to δ 12.50 ppm, and the proton in the methylene of -NCH_2- (**H5**) shifted downfield from 8.94 ppm to 9.06 ppm upon the addition of 1.0 equivalent of $Fe(NO_3)_3$to the **1b** solution. Additionally, the aryl protons (**H2**, **H3**, **H4**) also moved slightly to downfield, and the chemical shifts of the resonance peaks around δ 2.70–2.80 ppm (-SCH_2CH_2S-) shifted upfield by around 0.03 ppm. As shown in the IR spectrum (**Fig. S34**), the phenolic-OH absorption bands exhibited a significant blue-shift, blue-shift was also observed for the amide C–N from 1337 cm^{-1} to 1359 cm^{-1}, and signals in the region of 1350–1400 cm^{-1} assigned to -SCH_2 moved to high frequency. These results indicated that the O atom in phenolic-OH, N atom and S atom might be coordinated to Fe^{3+} ion.

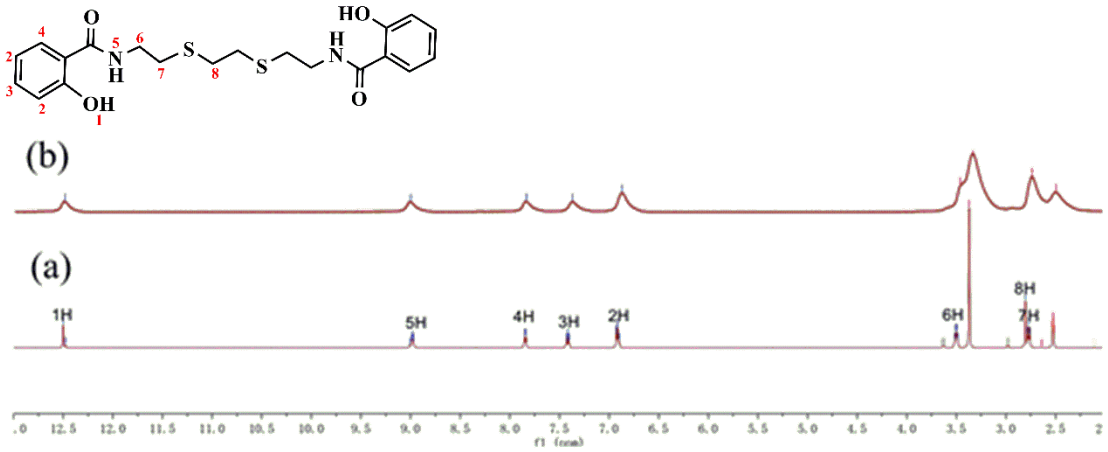

Fig.10. Partial ^1H NMR spectra of **1b** (7.5 mM) in DMSO-d_6: (a) free **1b**; (b) **1b** in the presence of $Fe(NO_3)_3$ (1.0 equiv.).

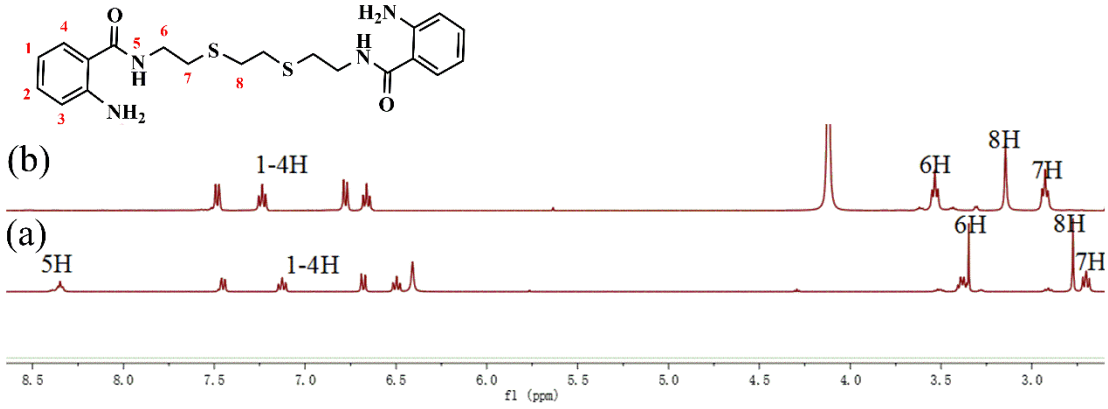

Fig. 11. Partial ^1H NMR spectra of **1c** (7.5 mM) in DMSO-d_6: (a) free **1c**; (b) **1c** in the presence of $HgCl_2$ (10equiv.).

Upon addition of 10 equiv. of $HgCl_2$ into **1c** solution, all protons in **1c** were shifted to downfield (**Fig. 11**). The aryl protons (**H1, H2, H3, H4**) were shifted obviously to downfield about 0.05 ppm. The aliphatic protons (**H8**) in the thioether group (-SCH_2CH_2S-) displayed considerable downfield shifts from 2.77 ppm to 3.15 ppm, which probably due to the interaction of S with Hg^{2+}. The other the aliphatic protons **H6** and **H7** were shifted to downfield about 0.16, 0.23 ppm respectively. In the IR spectrum (**Fig. S35, S36**), the characteristic absorption peak of $–NH_2$ (3469 cm^{-1}) on the benzene ring was changed in the presence of Hg^{2+}. These indicated that the N atom in amine and amide and S atom might be coordinated to Hg^{2+} ion.

According to ^1H NMR, the Job plot, fluorescence titration and ESI-mass analysis, we proposed possible structures of 1:1 complex of **1b** and Fe^{3+} and 1:2 complex of **1c** and Hg^{2+}. The computational study was conducted by using the density functional theory (DFT) combing natural bond orbital (NBO) analyses, and time-dependent (TD) DFT methods combining natural transition orbital (NTO) analyses in order to get a deep insight into the mechanism of the 'turn off' system for sensor **1b** and **1c**.

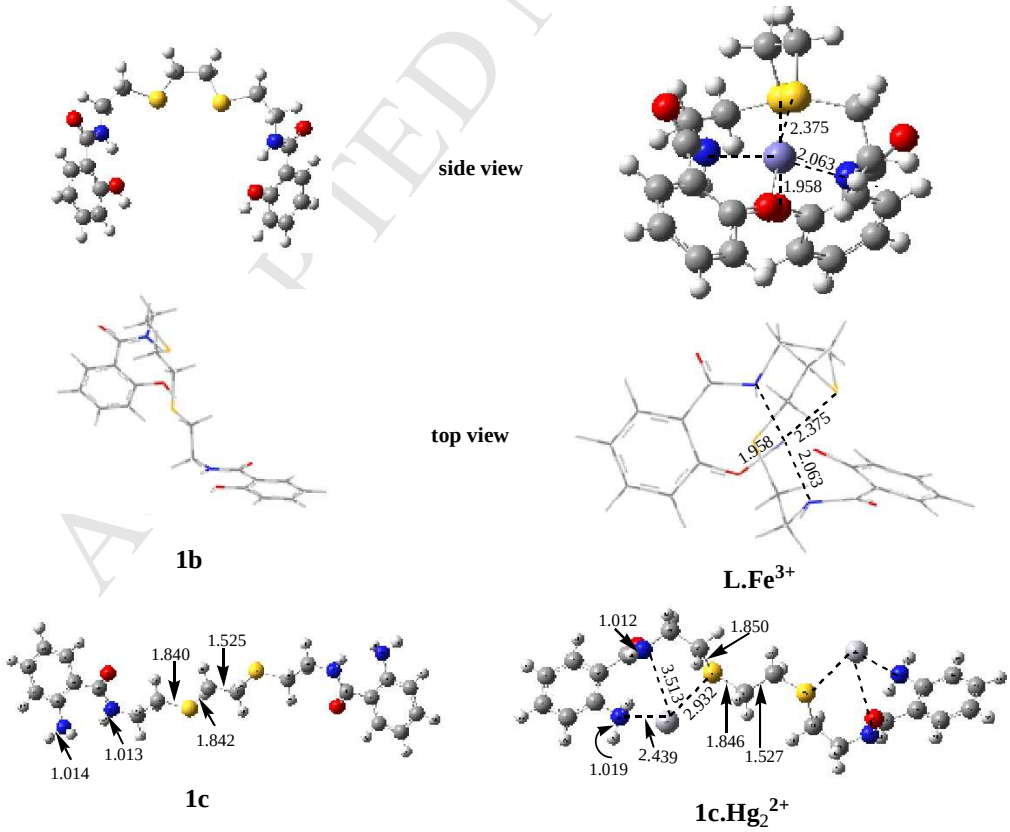

Fig.12. B3LYP and SMD salvation model optimized geometric structures for **1b** (**1b=H_2L**), **L.Fe^{3+}**, **1c** and **1c.Hg_2^{2+}** in aqueous solution, where the bond lengths are in the unit of Å. For clarity, both side views and top

views for both **1b** and **L.Fe^{3+}** are shown.

Table 1 Second Order Perturbation Theory Analysis of Fock Matrix in NBO Basis.

Donor NBO (i)	Acceptor NBO (j)	$E^{(2)}$ a) kcal/mol	E(j)-E(i)$^{b)}$ a.u.	F(i,j)$^{c)}$ a.u.
L.Fe^{3+} (1b = H_2L)				
LP (1) N8	LP*(4) Fe51	72.79	0.32	0.137
LP (1) N8	LP*(7) Fe51	24.77	0.59	0.115
LP (1) S11	LP*(5) Fe51	14.08	0.64	0.089
LP (1) S14	LP*(5) Fe51	12.67	0.65	0.085
LP (1) N17	LP*(4) Fe51	63.17	0.24	0.085
LP (1) N17	LP*(7) Fe51	25.65	0.59	0.116
LP (2) O19	LP*(5) Fe51	54.89	0.61	0.165
LP (2) O19	LP*(6) Fe51	55.86	0.73	0.184
LP (2) O28	LP*(5) Fe51	48.09	0.66	0.160
LP (3) O28	LP*(6) Fe51	66.75	0.77	0.206
BD (1) N8-H33	LP*(7) Fe51	14.13	0.88	0.102
BD (1) N17-H46	LP*(7) Fe51	14.03	0.88	0.102
1c.Hg_2^{2+}				
LP (2) S 9	LP*(6) Hg26	20.33	0.20	0.059
LP (1) N29	LP*(6) Hg26	21.33	0.26	0.068
LP (1) O30	LP*(8) Hg26	1.02	0.83	0.026
BD (1) N29-H56	LP*(1) Hg26	0.24	0.77	0.012
LP*(6) Hg 26	BD*(1) N29-H56	0.24	0.60	0.028
LP (2) S22	LP*(6) Hg27	20.56	0.20	0.059
LP (1) N25	LP*(6) Hg27	20.81	0.26	0.067
BD (1) N25-H54	LP*(7) Hg27	0.20	0.77	0.011
LP*(6) Hg27	BD*(1) N25-H54	0.23	0.60	0.028

a) $E^{(2)}$ denotes second order perturbation energy of hyperconjugative interactions between donor and acceptor i and j NBO orbitals; b) Energy difference between i and j NBO orbitals; c) The Fock matrix element i and j NBO orbitals

Available calculated results may support the energy and the charge transfer model for explaining the mechanism of the fluorescence quenching. As shown in **Fig. 12** and **Table S2**, which displayed the optimized geometric structures for **1b** (**1b**=**H_2L**), **L.Fe^{3+}**, **1c** and **1c.Hg_2^{2+}**, the Fe^{3+} ion was chelated through six coordination sites on **L** in **1b** (N atoms of two imino groups, O atoms of two phenol hydroxyls, and two S atoms), and each Hg^{2+} may be coordinated to **1c** through three sites (N atom of amino group, O atom of carbonyl group, and S atoms), where the lone pairs of the coordination atoms transferred to the metals. These binding situations were confirmed by larger second-order perturbation energy $E^{(2)}$ (which

means the energy of hyperconjugation interaction between donor NBO *i* and acceptor NBO j) between lone pair NBOs of each relevant S, N and O atoms and the unoccupied orbital of the metals than those between other sites in ligand and metals (shown in **Table 1**). Although weaker interactions existed between metals and ligand through other sites, the donation-back donation interaction mode was still clear. For example, the interaction energy $E^{(2)}$ between N-H bond of NH_2 and Hg^{2+} in **1c.Hg$_2^{2+}$** was just ca 0.24 kcal/mol, the donation of electron in each N-H bonding orbital to the virtual orbital of Hg^{2+} and back-donation of electron in Hg^{2+} to the anti-bonding orbital of N-H resulted in the weakening of the N-H bonds, which was in accordance with the elongation of the bond length from 0.1014 nm in **1c** to 0.1019 nm in **1c.Hg$_2^{2+}$**, and the decrease of the vibrational frequency from 3536.54 cm^{-1} in **1c** to 3512.26 cm^{-1} in **1c.Hg$_2^{2+}$**. Besides, optimized geometries and natural bond orbital (NBO) analyses showed that the interaction between N atom of imino group and metal ion in **L.Fe^{3+}** was fairly strong but very small in **1c.Hg$_2^{2+}$**. In addition, as shown in **Table S2,** on coordination of Fe^{3+} and Hg^{2+}, both the HOMO-LUMO gaps of two complexes **L.Fe^{3+}** and **1c.Hg$_2^{2+}$** became lower as compared to free **1b** and **1c**, respectively. From orbital interaction viewpoint, the smaller **H-L** gap was, the easier the electron was excited. This can explain what the electron density distribution of **1b** and **1c** were significantly influenced on complexation with Fe^{3+} and Hg^{2+}, respectively, due to the occurrence of the possible charge transfer processes between the ligands and the metal cations. The charge transfer could be further confirmed by the calculated natural electron density population. From **Table S3** we could find the decrease of the electron densities in all H atoms of **1c.Hg$_2^{2+}$** from those of **1c**, due to the charge transfer through complexation. This was in good agreement with the above-mentioned ^1H NMR spectroscopy observations.

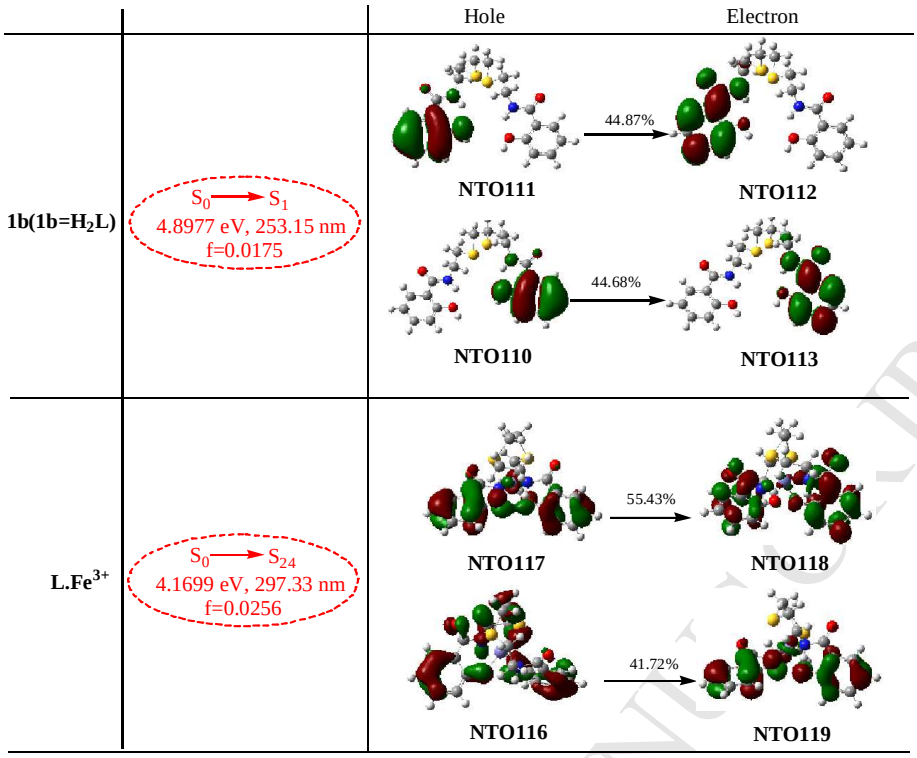

Fig. 13. The Natural transition orbital (NTO) pairs that mainly contribute to the intense singlet excitation states in UV-vis absorption for **1b** and its complex to Fe^{3+} in aqueous solution calculated by using TD-CAM-B3LYP and SMD salvation model, where f is oscillator strength

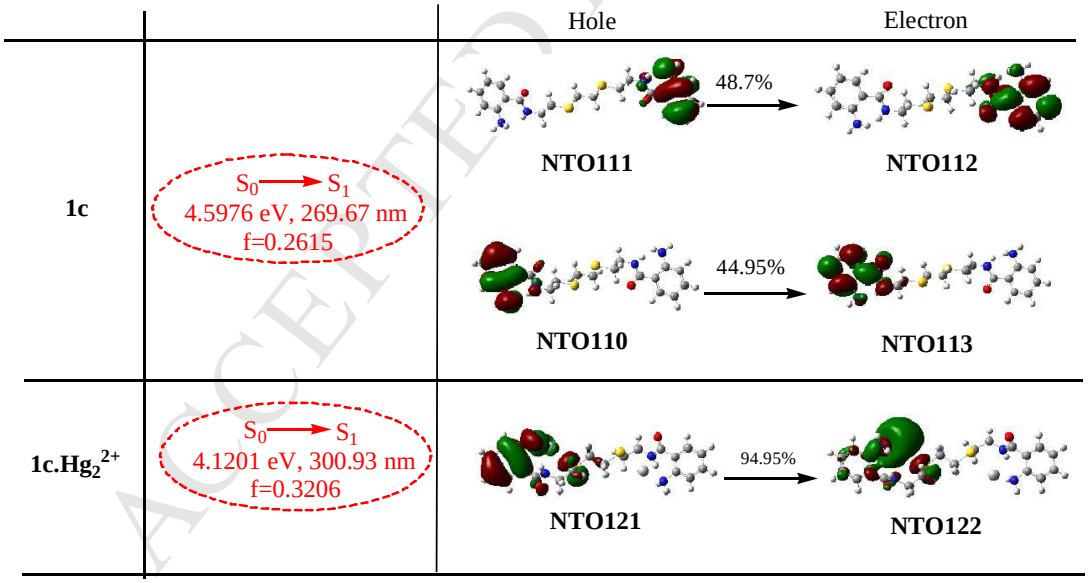

Fig. 14. The Natural transition orbital (NTO) pairs that mainly contribute to the intense singlet excitation states in UV-vis absorption for **1c** and its complex **1c. Hg_2^{2+}** in aqueous solution calculated by using TD-CAM-B3LYP and SMD salvation model, where f is oscillator strength

Furthermore, the energy and the charge transfer assumption could also be confirmed by TDDFT calculated results and the natural transition orbital (NTO)

distribution. From TD-CAM-B3LYP calculated results, each $s_0 \rightarrow s_1$ excitation for **1b**, **1c** and **1c.Hg$_2^{2+}$,** and $s_0 \rightarrow s_{24}$ excitation for **L.Fe^{3+}** could be assigned for the intense absorption of the corresponding molecules, respectively. Especially 297.33 nm of $s_0 \rightarrow s_{24}$ excitation for **L.Fe^{3+}** and 300.93 nm of $s_0 \rightarrow s_1$ excitation for **1c.Hg$_2^{2+}$** agree well with the experimental absorption of 298 and 313 nm (**Fig. S28**), respectively. While combining the observed short fluorescence lifetime (this may rule out the possibility of the intersystem crossing), the $s_1 \rightarrow s_0$ emission could be assigned for experimental fluorescence emission for relevant molecules. As shown in **Fig. 13, 14** and **Fig. S37**, where the optical excitations and emissions were mainly contributed by the transitions from the occupied (hole) NTOs to the unoccupied (electron) NTOs. Whatever $s_0 \rightarrow s_1$ and $s_0 \rightarrow s_{24}$ excitations or $s_1 \rightarrow s_0$ emission processes presented charge transfer character to some extent. Individually, the excitations of the four molecules could be depicted as follows. **1b** had the $s_0 \rightarrow s_1$ excitation energy of 4.8977 eV (253.15 nm) and the oscillator strength of 0.0175, which was mainly combined with two transitions between hole-electron NTO pairs. Since two NTO pairs predominantly localized on the central area of phenyl moiety, thus these transitions may be attributed as local excitation (LE) and intraligand charge transfer (ILCT). And **L.Fe^{3+}** had the $s_0 \rightarrow s_{24}$ excitation energy of 4.1699 eV (297.33 nm) and the oscillator strength of 0.0256. This excitation was also mainly attributed to the mixing of two transitions. In one transition, the hole NTO spread over the whole ligand backbone moiety, but the partner electron NTO predominantly localized on the partial area of ligand and the metal, thus this transition may be attributed as the mixing of ILCT and ligand to metal charge transfer (LMCT). From NTO distribution, another transition within this excitation may be assigned as the mixing of ILCT and metal to ligand charge transfer (MLCT). Then the $s_0 \rightarrow s_1$ excitation of **1c** (4.5976 eV, 269.67 nm, f=0.1680) was mainly combined with two NTO pairs transitions with ILCT and LE character. Moreover, the $s_0 \rightarrow s_1$ excitation of **1c.Hg$_2^{2+}$** (4.1201 eV, 300.93 nm, f=0.3206) was mainly contributed with one NTO pairs transition with the mixing of ILCT and LMCT obviously. Besides, the $s_1 \rightarrow s_0$ emission of **1c** (3.525 eV, 351.98 nm, f=0.2589) was predominantly LE and ILCT transition.

In a summary, on the one hand, it revealed that the present computational results along with the experimental data were efficient enough for exploring the interaction pattern. On the other hand, it confirmed that the fluorescence quenching in the presence of Fe^{3+} and Hg^{2+} may be due to the intramolecular charge transfer.

2.8 Practical application

To assess the practicability of **1b** and **1c** to real samples, they were used as the fluorescent sensors for the determination of Fe^{3+} and Hg^{2+} in drinking water. The detection results were displayed in **Table 2**. It was found the detected concentrations were close to the added concentration of ions. The results exhibited satisfactory recoveries and very low the relative standard deviation (RSD) values for both Fe^{3+} and Hg^{2+}. These results suggested that **1b** and **1c** could satisfactorily detect Fe^{3+} and Hg^{2+} in water samples, respectively.

Table 2 Determination of Fe^{3+} and Hg^{2+} in water samples

Sample	Added (μM)	Found (μM)	RSD. (%, n=3)	Recovery (%)
Fe^{3+}	0.100	0.109	2.2	109
	0.200	0.193	0.71	96.5
	0.300	0.280	1.0	93.3
Hg^{2+}	0.200	0.199	0.22	99.5
	0.400	0.400	2.2	100
	0.800	0.790	0.70	98.8

3. Conclusion

In summary, we have successfully designed and synthesized some thioether-linked bisbenzamide derivatives and switched their selectivity for metal ions by introducing different substituent groups into the benzene ring. The experiment data displayed the o-hydroxyl-attached probe **1b** exhibited selective 'turn-off' fluorescence response to Fe^{3+}, and the o-amino-attached probe **1c** selectively recognized Hg^{2+} by fluorescence quenching quickly. The binding stoichiometry was determined to be 1:1 for **1b**-Fe^{3+}, 1:2 for **1c**-Hg^{2+} based on Job's plot, fluorescent titration and ESI-MS. The detection limits of **1b** for Fe^{3+} and **1c** for Hg^{2+} were calculated as 0.3 μM and 0.5 μM by fluorescence titration, respectively. Moreover, combining SMD salvation model, theoretical calculations with B3LYP and NBO analyses, TD-CAM-B3LYP and NTO analyses, provided valuable confirmation to the experimental observation and rational recognition pattern, which supported the intramolecular charge transfer model for the mechanism of the fluorescence quenching. Both probes **1b** and **1c** were successfully

applied to the determination of Fe^{3+} or Hg^{2+} in drinking water. All these facts indicated that probe **1b** and **1c** could be served as simple, rapid, sensitive and selective chemosensors for Fe^{3+} and Hg^{2+} recognition, respectively. The presence sensing systems have great prospective in biomedical and environment detection.

4. Experimental

4.1 Reagents and materials

Unless stated otherwise, all analytical grad chemicals and solvents used in this paper were purchased from commercial vendors. Dimethyl formamide (DMF) was dried over 4 Å molecular sieves. Dichloromethane (DCM) was distilled from calcium hydride. Others were used directly without further purification. Ultrapure water was used to prepare stock solution (0.01 M) of $NaNO_3$, KNO_3, $Cu(NO_3)_2$, $Fe(NO_3)_2$, $Fe(NO_3)_3$, $MgNO_3$, $Ca(NO_3)_3$, $CrNO_3)_3$, $Ni(NO_3)_2$, $Zn(NO_3)_2$, $Co(NO_3)_2$, $HgCl_2$, $Pb(NO_3)_2$, $Cd(NO_3)_2$ and $AgNO_3$. Stock solutions (0.01M) of anions in water were prepared from NaCl, NaF, NaBr, $NaNO_3$, $NaNO_2$, $NaHCO_3$, Na_2CO_3, Na_2SO_4, Na_2SO_3, $NaHSO_3$, $Na_2S_2O_3$ and CH_3COONa. The stock solution of sensors was prepared by dissolving compounds **1a-g** in dimethyl sulfoxide (DMSO) and was used to prepare the DMSO aqueous solution.

4.2 Instrumentation

Melting points were determined with an X6 melting apparatus without correction. IR spectra in KBr were recorded on a Germany Bruker corporation VECTOR22 Fourier transform infrared spectrometer. ^1H NMR (600 MHz) and ^{13}C NMR (150 MHz) spectra were measured on a Varian Unity INOVA 600 NMR magnetic resonance spectrometer (TMS as internal standard). Mass spectrometry was recorded with a Finnigan LCQ mass spectrometer and an Agilent 1200 LC/MSD mass spectrometer. UV–Vis spectra were collected from a Shimadzu UV-2700 spectrophotometer at room temperature. The fluorescence spectra were obtained with RF-5301(PC) S spectrometer with a 1cm standard quartz cell. Fluorescence lifetimes were measured on Edinburgh FLS980 fluorescence spectrophotometer.

4.3 Synthesis and characterization of receptors

The compound **2** was prepared according to the reported procedure.[41,42] Sodium ethylate (3.13g, 46.1mmol) was dissolved in dry ethanol (40mL) and then cooled to 15°C. The cool solution was added to 2-aminoethanethiol hydrochloride (2.61g, 23.0 mmol). After the mixture was stirred for 15 min under nitrogen atmosphere, 1, 2-dibromoethane (1.0mL, 11.5mmol) was added and stirred for 4 h at 40°C.The mixture was filtered and evaporated under reduced pressure. The yellowish mass was dissolved in sodium hydroxide solution (5.0 g in 15mL water), and the resulting solution was kept in a refrigerator overnight. The solution was extracted with dichloromethane. The extract was evaporated to give 1.48 g (71%) of **2**. ^{1}H NMR (600 MHz, $CDCl_3$) δ 2.89 (t, *J* = 6.3 Hz, 2H), 2.74 (s, 2H), 2.66 (t, *J* = 6.3 Hz, 2H); ^{13}C NMR (147 MHz, CD_3OD): δ 41.53, 35.45, 32.71; LC-MS (ESI) m/z calculated for $[M+H]^+$ $C_6H_{16}N_2S_2^+$ 181.0800. Found 181.0810.

Synthesis of receptors **1a**-**1g**

The synthesis procedure **ii** was performed according to the literature method.[43,44] To an ice-cooled solution of the acid (2.5mmol) in dry CH_2Cl_2 (30mL), HOBt (0.40 g, 3mmol) and EDC (0.58 g, 3mmol) were added. The reaction mixture was stirred for 30 min, then compound **2** (0.18 g, 1mmol) in DCM (2mL) was added slowly. The resulting mixture was stirred at RT for 18h, and was monitored by TLC. After completion of the reaction, the mixture was extracted with CH_2CCl_2 (30mL), washed with aqueous $NaHCO_3$ (30mL) and H_2O (30mL). The organic layer was dried over Na_2SO_4 and removed by rotary evaporation. The extract was evaporated and the crude product was purified by column chromatography (DCM/ Methanol, 100:1 to 10:1) to afford pure product (**1a; 1b; 1c; 1e**). The receptors **1d**, **1f**, **1g** were prepared by the similar methodology as the above,[45,46] but HOBt and EDC were replaced with HBTU (1.42 g, 3.75mmol) and DIPEA (653µL,3.8 mmol).

1a:0.25 g, yield 63.3%; R_f = 0.7 (CH_2Cl_2/ Methanol = 10 : 1) ; m.p. 143-144°C; ^{1}H NMR (600 MHz, DMSO-d_6) δ12.48 (s, *J* = 6.24 Hz, 2H), 2.73 (s, 4H), 2.66 (t, *J* = 6.24 Hz, 4H); ^{13}C NMR (150 MHz, $CDCl_3$) : δ 167.54, 134.08, 131.38, 128.37, 126.79, 39.19, 31.33, 31.14; LC-MS (ESI) m/z calculated for $[M+H]^+$ $C_{20}H_{24}N_2O_2S_2^+$ 389.1310. Found 389.1340.

1b: 0.24 g, yield 62%; R_f = 0.6 (CH_2Cl_2/ Methanol = 10 : 1) ; m.p. 143-144°C; ^{1}H NMR (600 MHz, DMSO-d_6) δ 12.48 (s, 2H), 8.95 (t, *J* = 5.6 Hz, 2H), 7.82 (d, *J* = 7.9 Hz, 2H), 7.39 (t, *J* = 8.1 Hz, 2H), 6.93 – 6.85 (m, 4H), 3.48 (q, *J* = 6.6 Hz, 4H), 2.78 (s, 4H), 2.74 (t, *J* = 7.1 Hz, 4H); ^{13}C NMR (150 MHz, DMSO-d_6) : δ 169.47, 160.56, 134.34, 128.43, 119.25, 118.03, 115.89, 40.61, 40.47, 40.32, 40.18, 40.04, 31.73, 30.87; LC-MS (ESI) m/z calculated for $[M+H]^+$ $C_{20}H_{24}N_2O_4S_2^+$ 421.1201. Found 421.1208.

1c: 0.25 g, yield 58%; R_f = 0.72 (CH_2Cl_2/ Methanol = 10 : 1) ; m.p. 143-144°C; ^{1}H NMR (600 MHz, DMSO-d_6) δ 8.35 (t, *J* = 5.8 Hz, 2H), 7.45 (d, *J* = 8.1 Hz, 2H), 7.13 (t, *J* = 7.6 Hz, 2H), 6.68 (d, *J* = 8.2 Hz, 2H), 6.50 (t, *J* = 7.5 Hz, 2H), 6.41 (s, 5H), 3.38 (q, *J* = 6.6 Hz, 4H), 2.77 (s, 4H), 2.70 (t, *J* = 7.2 Hz, 4H);^{13}C NMR (150 MHz, DMSO-d_6) : δ 168.94, 168.83, 149.62, 149.59, 131.71, 131.66, 128.00, 127.95, 116.34, 114.52, 114.42, 39.93, 38.95, 38.82, 38.38, 37.20, 31.04, 30.42. LC-MS (ESI) m/z calculated for $[M+H]^+$ $C_{20}H_{26}N_4O_2S_2^+$ 419.1526. Found 419.1530.

1d: 0.25 g, yield 63%; R_f = 0.8(CH_2Cl_2/ Methanol = 10 : 1) ; m.p. 143-144°C; ^{1}H NMR (600 MHz, $CDCl_3$) δ 8.33 (s, 2H), 8.19 (d, *J* = 7.6 Hz, 2H), 7.45 (d, *J* = 8.4 Hz, 2H), 7.07 (dt, *J* = 11.0, 5.6 Hz, 2H), 6.97 (dd, *J* = 8.2, 3.7 Hz, 2H), 3.98 (d, *J* = 3.5 Hz, 6H), 3.83-3.66 (m, 4H), 2.99-2.77 (m, 8H). ^{13}C NMR (150 MHz, $CDCl_3$) : δ 165.37, 157.53 , 132.87, 132.16 , 121.23 , 111.31 , 55.99 , 39.05 , 38.33 , 38.00 , 31.82.LC-MS (ESI) m/z calculated for $[M+H]^+$ $C_{22}H_{28}N_2O_4S_2^+$ 449.1550. Found 449.1549.

1e: 0.25 g, yield 63%; R_f = 0.5(CH_2Cl_2/ Methanol = 10 : 1) ; m.p. 143-144°C; ^{1}H NMR (584 MHz, DMSO-d_6) δ 8.45 (t, *J* = 5.9 Hz, 2H), 7.75 (d, *J* = 7.6 Hz, 2H), 7.55 (t, *J* = 7.5 Hz, 2H), 7.50 (t, *J* = 7.6 Hz, 3H), 7.40 (d, *J* = 7.4 Hz, 2H), 3.36 (d, *J* = 7.0 Hz, 4H), 2.78 (s, 4H), 2.70 (t, *J* = 7.4 Hz, 4H);^{13}C NMR (150MHz, DMSO-d_6) : δ 169.22, 168.57, 138.97, 131.81, 131.40, 129.84, 129.82, 128.18, 40.59, 31.73, 30.68. LC-MS (ESI) m/z calculated for $[M+H]^+$ $C_{22}H_{24}N_2O_6S_2^+$ 477.1155. Found 477.1160.

1f: 0.25 g, yield 63%; R_f = 0.65 (CH_2Cl_2/ Methanol = 10 : 1) ; m.p. 143-144°C; ^{1}H NMR (600 MHz, DMSO-d_6) δ 8.58 (d, *J* = 5.9 Hz, 2H), 7.65 (dd, *J* = 8.0, 3.9 Hz, 2H), 7.39 (ddd, *J* = 25.7, 13.4, 6.6 Hz, 4H), 3.40 (q, *J* = 6.4 Hz, 4H), 2.80 (d, *J* = 4.3

Hz, 4H), 2.72 (t, *J* = 6.8 Hz,4H).^{13}C NMR (150 MHz, DMSO-d_6): δ 167.94, 167.86, 139.64, 139.60, 134.34, 133.33, 131.50, 129.38, 128.33, 128.17, 119.54, 40.59, 31.72, 30.93. LC-MS (ESI) m/z calculated for $[M+H]^+$ $C_{20}H_{22}Br_2N_2O_2S_2^+$ 546.9540. Found 546.9542.

1g: 0.25 g, yield 63 %; R_f = 0.55 (CH_2Cl_2/ Methanol = 10 : 1) ; m.p. 143-144°C; ^{1}H NMR (600 MHz, DMSO-d_6) δ 8.44 (s, 2H),7.63 (t, *J* = 7.7 Hz, 2H), 7.53 (q, *J* = 7.2 Hz,2H), 7.28 (q, *J* = 8.2, 7.2 Hz, 2H), 3.43 (q, *J* = 6.8 Hz, 4H), 2.78 (s, 4H), 2.72 (t, *J* = 7.3 Hz, 4H).^{13}C NMR (150 MHz, $CDCl_3$) : δ 163.28, 163.26, 161.24, 159.55, 133.16, 133.10, 131.68, 124.58, 124.56, 120.81, 120.72, 115.92, 115.75, 76.88, 76.66, 39.16, 38.62, 37.42, 31.59, 31.33. LC-MS (ESI) m/z calculated for $[M+H]^+$ $C_{20}H_{22}F_2N_2O_2S_2^+$ 425.1130. Found 425.1135.

4.4 Calculation of the relative fluorescence quantum yield

Fluorescence quantum yield was determined by using quinine sulphate (Φs =0.546 in 0.1 M H2SO4) as a fluorescence standard. The quantum yield was calculated using the following equation:

$$\Phi x = \Phi s(AsFx/AxFs)(nx/ns)^2$$

Where Φx is the fluorescence quantum yield, A is the absorbance at the excitation wavelength, F is the integrated area under the corrected emission curve, and n is the refractive index of the medium. Subscripts S and X refer to the standard and to the unknown, respectively.

4.5 Computational methodology

Density functional theory (DFT) method with B3LYP functional[47,48] had been utilized to optimize geometric structures of molecules **1b** (**1b**=**H_2L**), **1c** and their complexes **L.Fe^{3+}**, and **1c.Hg_2^{2+}** in the lowest singlet spin state s_0, then vibrational analyses had been done by frequency calculations to verify that the geometries obtained are minima or not and obtain vibrational spectra. To get more detailed information on the chemical bonds and bonding interaction within all four molecules, natural bonding orbital (NBO) calculations[49,50] were carried out using B3LYP method on the optimized geometries. Based on the optimized geometries, vertical electronic excitation energies and absorption spectra were calculated with time-dependent (TD)

DFT, TD-CAM-B3LYP method.[51] The geometries for the first excited singlet states s_1 of **1b** and **1c** were optimized with TD-CAM-B3LYP method to obtain their fluorescence emission energies and spectra. In order to analyze the nature of absorption and emission, natural transition orbital (NTO) analyses were performed based on the TDDFT calculations and the calculated transition density matrices[52]. In all calculations, the salvation effect was considered with SMD salvation model[53] and water media; the 6-31G (d, p) basis set for the atoms C, N, O, S and H, and relativistic pseudo-potential LanL2dz basis set for Fe and Hg were selected. All calculations were performed with Gaussian 09 program[54].

Acknowledgments

This work was supported by the National Natural Science Foundation of China (Grant 21575035), and Foreign Science and Technology Cooperation Fund of Hubei province, China (2015BHE025).

Appendix A. Supplementary data

The following is the supplementary data related to this article:

Supplementary data associated with this article (^{1}H, ^{13}C NMR and MS spectra).

References

1. Boonkitpatarakul, K.; Wang, J.; Niamnont, N.; Liu, B.; McDonald, L.; Pang, Y.; Sukwattanasinitt, M. *ACS Sensors* **2016,** *1*, 144-150.
2. Han, X.; Wang, D.-E.; Chen, S.; Zhang, L.; Guo, Y.; Wang, J. *Anal. Methods* **2015,** *7*, 4231-4236.
3. Yang, M.; Meng, W.; Ding, Q.; Su, N.; Liu, X.; Zhang, M.; Yang, B. *New J. Chem.* **2015,** *39*, 4790-4795.
4. Ding, J.; Li, H.; Wang, C.; Yang, J.; Xie, Y.; Peng, Q.; Li, Q.; Li, Z. *ACS Appl Mater Interfaces* **2015,** *7*, 11369-76.
5. Kaushik, R.; Ghosh, A.; Singh, A.; Gupta, P.; Mittal, A.; Jose, D. A. *ACS Sensors* **2016,** *1*, 1265-1271.
6. Liu, T.; Wan, X.; Yao, Y. *Sensors and Actuators B: Chemical* **2018,** *254*, 1094-1100.
7. Wang, Z.; Yang, J.; Yang, Y.; Fang, H.; Xu, X.; Rui, J.; Su, F.; Xu, H.; Wang, S. *RSC Adv.* **2017,** *7*, 33263-33272.
8. Wu, W.; Chen, A.; Tong, L.; Qing, Z.; Langone, K. P.; Bernier, W. E.; Jones, W. E., Jr. *ACS Sens* **2017**.
9. Wu, X.; Zhang, S.; Niu, Q.; Li, T. *Tetrahedron Letters* **2016,** *57*, 3407-3411.
10. Foster, K. L.; Stern, G. A.; Pazerniuk, M. A.; Hickie, B.; Walkusz, W.; Wang, F.; Macdonald, R. W. *Environ Sci Technol* **2012,** *46*, 12952-9.
11. Huang, X.; Li, M.; Friedli, H. R.; Song, Y.; Chang, D.; Zhu, L. *Environ Sci Technol* **2011,** *45*, 9442-8.

12. Lambert, K. F.; Evers, D. C.; Warner, K. A.; King, S. L.; Selin, N. E. *Environ Res* **2012,** *119*, 132-42.
13. Carter, K. P.; Young, A. M.; Palmer, A. E. *Chem Rev* **2014,** *114*, 4564-601.
14. Chen, X.; Pradhan, T.; Wang, F.; Kim, J. S.; Yoon, J. *Chem Rev* **2012,** *112*, 1910-56.
15. Comin-Colet, J.; Lainscak, M.; Dickstein, K.; Filippatos, G. S.; Johnson, P.; Luscher, T. F.; Mori, C.; Willenheimer, R.; Ponikowski, P.; Anker, S. D. *Eur Heart J* **2013,** *34*, 30-8.
16. Zheng, M.; Tan, H.; Xie, Z.; Zhang, L.; Jing, X.; Sun, Z. *ACS Appl Mater Interfaces* **2013,** *5*, 1078-83.
17. Bozkurt, E.; Gul, H. I. *Sensors and Actuators B: Chemical* **2017**.
18. Liu, Y.; Shen, R.; Ru, J.; Yao, X.; Yang, Y.; Liu, H.; Tang, X.; Bai, D.; Zhang, G.; Liu, W. *RSC Adv.* **2016,** *6*, 111754-111759.
19. Shu, W.; Yan, L.; Liu, J.; Wang, Z.; Zhang, S.; Tang, C.; Liu, C.; Zhu, B.; Du, B. *Industrial & Engineering Chemistry Research* **2015,** *54*, 8056-8062.
20. Yang, X.; Liu, X.; Li, Y.; Wu, F.; Mao, J.; Yuan, Y.; Cui, Y.; Sun, G.; Zhang, G. *Biosens Bioelectron* **2016,** *80*, 288-93.
21. Ahmad Wani, M.; Thakur, N.; Pandey, M. D.; Pandey, R. *New Journal of Chemistry* **2017,** *41*, 10000-10008.
22. Hirayama, T.; Nagasawa, H. *Journal of Clinical Biochemistry and Nutrition* **2017,** *60*, 39-48.
23. Jiang, C.; Wang, M.; Wang, Y.; Tang, X.; Zhang, Y.; Zhang, H.; Ma, L.; Wang, J. *Tetrahedron Letters* **2017,** *58*, 2560-2565.
24. Ju, H.; Chang, D. J.; Kim, S.; Ryu, H.; Lee, E.; Park, I. H.; Jung, J. H.; Ikeda, M.; Habata, Y.; Lee, S. S. *Inorg Chem* **2016,** *55*, 7448-56.
25. Maity, A.; Sil, A.; Nad, S.; Patra, S. K. *Sensors and Actuators B: Chemical* **2018,** *255*, 299-308.
26. Wu, B.; Xu, L.; Wang, S.; Wang, Y.; Zhang, W. *Polym. Chem.* **2015,** *6*, 4279-4289.
27. Xu, D.; Tang, L.; Tian, M.; He, P.; Yan, X. *Tetrahedron Letters* **2017,** *58*, 3654-3657.
28. Li, J.; Yim, D.; Jang, W. D.; Yoon, J. *Chem Soc Rev* **2017,** *46*, 2437-2458.
29. Zhu, M.; Yuan, M.; Liu, X.; Xu, J.; Lv, J.; Huang, C.; Liu, H.; Li, Y.; Wang, S.; Zhu, D. *Organic Letters* **2008,** *10*, 1481-1484.
30. Sui, B.; Tang, S.; Liu, T.; Kim, B.; Belfield, K. D. *ACS Appl Mater Interfaces* **2014,** *6*, 18408-12.
31. Dodani, S. C.; Leary, S. C.; Cobine, P. A.; Winge, D. R.; Chang, C. J. *J Am Chem Soc* **2011,** *133*, 8606-16.
32. Domaille, D. W.; Zeng, L.; Chang, C. J. *Journal of the American Chemical Society* **2010,** *132*, 1194-1195.
33. Xu, C.; Liu, W.; Qin, W. *J Phys Chem A* **2011,** *115*, 4288-98.
34. Zhao, B.; Xu, Y.; Fang, Y.; Wang, L.; Deng, Q. *Tetrahedron Letters* **2015,** *56*, 2460-2465.
35. Du, J.; Fan, J.; Peng, X.; Li, H.; Wang, J.; Sun, S. *J Fluoresc* **2008,** *18*, 919-24.
36. Lee, S. J.; Jung, J. H.; Seo, J.; Yoon, I.; Park, K.-M.; Lindoy, L. F.; Lee, S. S. *Organic Letters* **2006,** *8*, 1641-1643.
37. Liao, G.; Zheng, C.; Xue, D.; Fan, C.; Liu, G.; Pu, S. *RSC Adv.* **2016,** *6*, 34748-34753.
38. Bozkurt, E.; Arık, M.; Onganer, Y. *Sensors and Actuators B: Chemical* **2015,** *221*, 136-147.
39. Erdemir, S.; Yuksekogul, M.; Karakurt, S.; Kocyigit, O. *Sensors and Actuators B: Chemical* **2017,** *241*, 230-238.
40. Roy, N.; Nath, S.; Dutta, A.; Mondal, P.; Paul, P. C.; Singh, T. S. *RSC Adv.* **2016,** *6*, 63837-63847.
41. Choudhury, S. B.; Ray, D.; Chakravorty, A. *Inorganic Chemistry* **1991,** *30*, 4354-4360.

42. Nutthanara, P.; Ngeontae, W.; Imyim, A.; Kreethadumrongdat, T. *Journal of Applied Polymer Science* **2009**, n/a-n/a.
43. Musiol, R.; Tabak, D.; Niedbala, H.; Podeszwa, B.; Jampilek, J.; Kralova, K.; Dohnal, J.; Finster, J.; Mencel, A.; Polanski, J. *Bioorg Med Chem* **2008,** *16*, 4490-9.
44. Taj, R.; Sorensen, J. L. *Tetrahedron Letters* **2015,** *56*, 7108-7111.
45. Bajaj, M.; Mamidyala, S. K.; Zuegg, J.; Begg, S. L.; Ween, M. P.; Luo, Z.; Huang, J. X.; McEwan, A. G.; Kobe, B.; Paton, J. C.; McDevitt, C. A.; Cooper, M. A. *ACS Chem Biol* **2015,** *10*, 1511-20.
46. Peng, X.; He, H.; Xia, J.; Lou, Z.; Chang, G.; Zhang, X.; Wang, S. *Tetrahedron Letters* **2014,** *55*, 3541-3544.
47. Becke, A. D. *Physical Review A* **1988,** *38*, 3098-3100.
48. Lee, C.; Yang, W.; Parr, R. G. *Physical Review B* **1988,** *37*, 785-789.
49. Glendening, E. D.; Landis, C. R.; Weinhold, F. *Wiley Interdisciplinary Reviews: Computational Molecular Science* **2012,** *2*, 1-42.
50. Reed, A. E.; Curtiss, L. A.; Weinhold, F. *Chemical Reviews* **1988,** *88*, 899-926.
51. Yanai, T.; Tew, D. P.; Handy, N. C. *Chemical Physics Letters* **2004,** *393*, 51-57.
52. Martin, R. L. J. Chem. Phys., 2003, 118, 4775-4777.
53. Marenich, A. V. ; Cramer, C. J.; Truhlar, D. G. J. Phys. Chem. B, 2009,113, 6378-
54 Gaussian 09, Revision E.01, Frisch, M. J.; Trucks, G. W.; Schlegel, H. B.; Scuseria, G. E.; Robb, M. A.; Cheeseman, J. R.; Scalmani, G.; Barone, V.; Mennucci, B.; Petersson, G. A.; Nakatsuji, H.; Caricato, M.; Li, X.; Hratchian, H. P.; Izmaylov, A. F.; Bloino, J.; Zheng, G.; Sonnenberg, J. L.; Hada, M.; Ehara, M.; Toyota, K.; Fukuda, R.; Hasegawa, J.; Ishida, M.; Nakajima, T.; Honda, Y.; Kitao, O.; Nakai, H.; Vreven, T. ; Montgomery, Jr., J. A.; Peralta, J. E.; Ogliaro, F.; Bearpark, M.; Heyd, J. J. ; Brothers, E.; Kudin, K. N.; Staroverov, V. N.; Keith, T.; Kobayashi, R.; Normand, J.; Raghavachari, K.; Rendell, A.; Burant, J. C.; Iyengar, S. S.; Tomasi, J.; Cossi, M.; Rega, N.; Millam, J. M.; Klene, M.; Knox, J. E.; Cross, J. B.; Bakken, V.; Adamo, C.; Jaramillo, J.; Gomperts, R.; Stratmann, R. E.; Yazyev, O.; Austin, A. J.; Cammi, R.; Pomelli, C.; Ochterski, J. W.; Martin, R. L.; Morokuma, K.; Zakrzewski, V. G.; Voth, G. A.; Salvador, P.; Dannenberg, J. J.; Dapprich, S.; Daniels, A. D.; Farkas, O.; Foresman, J. B.; Ortiz, J. V.; Cioslowski, J. and Fox, D. J. Gaussian, Inc., Wallingford CT, 2013.